Variable-Parameter T-Circuit-Based IPT System Charging Battery With Constant Current or Constant Voltage Output

Yang Chen, *Student Member, IEEE*, Mingxuan Li, Bin Yang, Shuxin Chen, *Student Member, IEEE*, Qiao Li, Zhengyou He, *Senior Member, IEEE*, and Ruikun Mai, *Member, IEEE*

***Abstract*—Load-independent output characteristics of inductive power transfer (IPT) systems are increasingly popular in battery charging. This paper proposes a novel variable-parameter T-circuit (VT) for an IPT system charging a battery with constant current (CC) or constant voltage (CV) output. The VT can transfer a CC/CV input to a CC or CV output by using an ac switch and a passive component (inductor or capacitor). An IPT system with a VT for CC–CV charging can reduce the number of passive components and ac switches. Besides, the proposed VT merits more design freedom of charge current/voltage with the constraints imposed by the loosely coupled transformer parameters compared to that of the traditional one. In addition, there are three kinds of VTs for various IPT charging systems with different requirements. A 400 W laboratory-scale prototype with a 150 mm air gap was built to verify the theoretical analyses. Both electronic load and lead-acid battery are utilized to verify the charging profile of the proposed method. The experimental results of the IPT system indicate that the fluctuation of the charging current in CC mode is less than 2%, and the change rate of charging voltage in CV mode is within 2.9%. The maximum overall efficiency 93.93% of the charging system is achieved from a dc 110 V input to a dc 100 V output.**

***Index Terms*—Constant current (CC), constant voltage (CV), inductive power transfer (IPT), T-circuit, variable parameter.**

I. Introduction

INDUCTIVE power transfer (IPT) technology [1]–[3] can deliver energy from power sources to loads through magnetic coupling without contact, realizing electrical and mechanical isolation. Due to its inherent advantages of safety, convenience, and flexibility, it is widely adopted in many applications such as consumer electronics [3], [4], electric bicycles [5], [6], electric vehicles [7], [8], etc. In IPT charging applications, it is of significance to maintain constant current (CC) or constant voltage (CV) output, because CC–CV charging is one of the most efficient and commonly used methods [9]. During the whole charging process, the battery equivalent load R_{B}, defined as the ratio of charging voltage v_{B} to charging current i_{B} ($R_{\mathrm{B}} = v_{\mathrm{B}}/i_{\mathrm{B}}$), changes in a wide range, which can vary from several ohms to hundreds of ohms.

A. Related Works

A lot of effort has been carried out on how to achieve CC–CV charging. Generally, these approaches can be roughly classified into two categories.

1) Control Schemes for CC–CV Charging [10]–[12], [14], [15]: In [10], phase shift control is used to modulate the output voltage of the high-frequency inverter to attain the required charging current or voltage. Besides, IPT charging systems can operate at two different frequencies with load-independent output current or voltage [11], [12], but a stability issue may occur because of the frequency bifurcation phenomenon [13]. Buja *et al.* [14] and Li *et al.* [15] employ dc–dc converters on the primary side or secondary side to charge electric city cars and sightseeing cars. These control methods can let IPT systems operate with required output at the expense of a wide range of input modulation index and/or complicated control circuitry, suffering from control complexity and compromising converter efficiency [16]. Moreover, it is not easy to design the proportional–integral–derivative (PID) parameters for an IPT system with a wide range load because once the load changes the PID parameters should be adjusted and reselected according to the new load for good performance [17]. If an IPT system has an inherent load-independent transfer function, it can simplify control schemes, narrow down the range of input modulation index, or even cancel control [16].

2) Compensation Topologies for CC–CV Charging [9], [19]–[24]: Compensation topologies with CC or CV outputs [16], [18] draw much attention of the researchers because these topologies are equipped with native load-independent transfer functions. It can combine CC-output topologies and CV-output topologies to form hybrid topologies for CC–CV

Manuscript received December 31, 2018; revised March 28, 2019 and May 10, 2019; accepted June 1, 2019. Date of publication June 4, 2019; date of current version November 12, 2019. This work was supported in part by the National Key Research and Development Program of China under Grant 2017YFB1201002, in part by the National Natural Science Foundation of China under Grant 51677155, in part by the National Science Fund for Distinguished Young Scholars under Grant 51525702, in part by the Cultivation Program for the Excellent Doctoral Dissertation of Southwest Jiaotong University under Grant 2016310066, and in part by the Scholarship under the State Scholarship Fund of China Scholarship Council under Grant 201807000025. Recommended for publication by Associate Editor W.-H. Ki. *(Corresponding author: Ruikun Mai.)*

Y. Chen, M. Li, B. Yang, Q. Li, Z. He, and R. Mai are with the School of Electrical Engineering, Southwest Jiaotong University, Sichuan 611756, China (e-mail: yang.chen92@foxmail.com; 2495759072@qq.com; 546867343@qq.com; 574143439@qq.com; hezy@home.swjtu.edu.cn; mairk@swjtu.edu.cn).

S. Chen is with the School of Electrical and Electronic Engineering, Nanyang Technological University, Singapore 639798 (e-mail: chen1095@e.ntu.edu.sg).

Color versions of one or more of the figures in this paper are available online at http://ieeexplore.ieee.org.

Digital Object Identifier 10.1109/TPEL.2019.2920948

charging. In [19], two kinds of hybrid topologies [series–series (SS) and inductor–capacitor–inductor/series (*LCL*/S), series–parallel (SP), and inductor–capacitor–inductor/parallel (*LCL*/P)] are proposed for battery charging applications. In order to cancel the wireless communication link between the primary and secondary sides and to charge massive loads simultaneously, Mai *et al.* [20] propose a hybrid topology switching between SS and series/inductor–capacitor–capacitor (S/*LCC*) topologies. Besides, a dual-topology, which involves three capacitors, four switches, and a center-tapped loosely coupled transformer (LCT), alters from SS to SP topologies to manipulate battery load profile [21]. The work by Li *et al*. [22] uses three-coil based on SSS and S/S/*LCC* topologies to realize CC and CV outputs. Aiming at a compact structure, a new variable coil structure consisting of three-layer coils, i.e., two bipolar coils and one unipolar coil on the primary side is provided for CC–CV charging [23]. Moreover, a hybrid and reconfigurable IPT system with high-misalignment tolerance is reported in [9], where the hybrid and reconfigurable topology can tolerate misalignment and achieve battery charging. However, either output currents or output voltages of these methods mentioned above are only related to LCT parameters (mutual inductance and self-inductances), which limits the design of charge current I_{B} or charge voltage V_{B}. With fixed LCT parameters, there are two cases, i.e., CASE ①: if the voltage/current gain is only related to the LCT parameters, the output voltage/current is fixed; CASE ②: If the voltage/current gain is not just associated with the LCT parameters and has design freedom on parameters, the output voltage/current can be changed by adjusting other circuitry parameters even with fixed LCT parameters. For CASE ②, it is defined that the output voltage/current has design freedom with the constraints of LCT parameters in this paper. If the input-to-output transfer function of a converter has design freedom with the constraints imposed by the LCT parameters, it can help mitigate the design requirements of the LCT. In order to solve the problem, a hybrid topology with configurable charge current and charge voltage is proposed by Chen *et al*. in [24], using two/three T-circuits to meet charging profiles. Nevertheless, the topology is complex as it consists of five capacitors, two inductors, and two switches. It is better to employ fewer passive components (inductors or capacitors) in systems for cost reduction. Moreover, all the hybrid topologies for CC–CV charging utilize at least two ac switches to alter the charging mode, and each switch comprise two MOSFETs or insulated gate bipolar transistors [20]. If one switch is reduced, two semiconductor devices can be saved at once. Therefore, it is of importance to reduce the number of passive components and ac switches used in hybrid topologies for CC–CV charging.

B. Contributions

The main contributions of this paper are summarized as follows.

1) *Proposing novel variable-parameter T-circuits:* Traditional T-circuit is famous for its reciprocity between a voltage source and a current source. But at least two cascaded T-circuits are required to transfer a CC (CV) input to a CC (CV) output. The proposed variable-parameter T-circuit (VT) can make it with the help of one T-circuit, reducing the number of passive components. Besides, it can also transfer CC (CV) input to CV (CC) output. By adding an ac switch and a passive component (an inductor or a capacitor), the VT can transfer a CC/CV input to a CC or CV output. The T-circuit with variable parameter has a native load-independent transfer function, which can simplify control schemes.
2) *Improving the design freedom of charge current and charge voltage:* The charge currents or charge voltages of conventional hybrid topologies for CC–CV charging are only related to the LCT parameters, namely, once the parameters of LCT are fixed, the output current and voltage of VT are hard to change unless using another set of LCT with different parameters. In practice, the space for an LCT is always limited, which makes it tough to manufacture an LCT in view of all requirements [25]. The proposed VT can let the charge current and voltage of the IPT system have design freedom with the constraints of the LCT parameters.
3) *Supporting various IPT charging systems with different requirements:* During the derivation of VT, three possible variable parameters of the VT, which can be altered between CC and CV modes, are brought out. These ways of altering different variable parameters with different transfer function can be employed for various IPT charging systems with different requirements.

The rest of the paper is organized as follows. In Section II, VT is systematically analyzed with a voltage source and current source. Section III discusses an IPT system using VT for CC–CV charging. Experimental results and comparisons with other methods are presented in Section IV to validate the proposed method. Finally, conclusions are drawn in Section V.

II. Analysis of T-Circuit

A. Analysis of a T-Circuit Driven by a Voltage Source

As shown in Fig. 1, a T-circuit is driven by a sinusoidal voltage source with angular frequency ω, where $\omega = 2\pi f$ and f is the operating frequency. $\dot{V}_{\mathrm{in}}$ ($\dot{V}_{\mathrm{out}}$) and $\dot{I}_{\mathrm{in}}$ ($\dot{I}_{\mathrm{out}}$) are the phasors of the input (output) voltage and current. R_{T} and Z_{in} are the load resistance and input impedance of the T-circuit, respectively. Z_1, Z_2, Z_3 are the corresponding impedances of each component (inductor or capacitor), i.e.

$$Z_1 = jX_1, \quad Z_2 = jX_2, \quad Z_3 = jX_3. \tag{1}$$

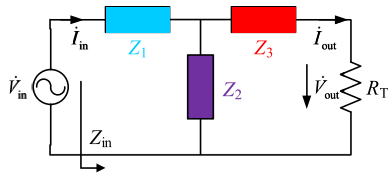

Fig. 1. T-circuit driven by a voltage source.

According to Kirchhoff's voltage law (KVL), the T-circuit can be expressed by

$$\begin{bmatrix} \dot{V}_{\rm in} \\ 0 \end{bmatrix} = \begin{bmatrix} Z_1+Z_2 & -Z_2 \\ -Z_2 & Z_2+Z_3+R_{\rm T} \end{bmatrix} \begin{bmatrix} \dot{I}_{\rm in} \\ \dot{I}_{\rm out} \end{bmatrix}. \quad (2)$$

After solving (2), the input and output currents ($\dot{I}_{\rm in}$ and $\dot{I}_{\rm out}$) can be derived as follows:

$$\begin{cases} \dot{I}_{\rm in} = \frac{Z_2+Z_3+R_{\rm T}}{Z_1Z_2+Z_1Z_3+Z_2Z_3+(Z_1+Z_2)R_{\rm T}}\dot{V}_{\rm in} \\ \dot{I}_{\rm out} = \frac{Z_2}{Z_1Z_2+Z_1Z_3+Z_2Z_3+(Z_1+Z_2)R_{\rm T}}\dot{V}_{\rm in}. \end{cases} \quad (3)$$

Then, the output voltage $\dot{V}_{\rm out}$ of load resistance $R_{\rm T}$ is given by

$$\dot{V}_{\rm out} = \frac{Z_2R_{\rm T}}{Z_1Z_2+Z_1Z_3+Z_2Z_3+(Z_1+Z_2)\,R_{\rm T}}\dot{V}_{\rm in}. \quad (4)$$

The transfer admittance $G_{\rm VI}$ of the T-circuit is denoted as the ratio of the output current $\dot{I}_{\rm out}$ to the input voltage $\dot{V}_{\rm in}$, namely

$$G_{\rm VI} = \left|\frac{\dot{I}_{\rm out}}{\dot{V}_{\rm in}}\right| = \left|\frac{Z_2}{Z_1Z_2+Z_1Z_3+Z_2Z_3+(Z_1+Z_2)\,R_{\rm T}}\right|. \quad (5)$$

Likewise, the voltage gain $G_{\rm VV}$, which is defined as the ratio between the output voltage $\dot{V}_{\rm out}$ and the input voltage $\dot{V}_{\rm in}$, is shown as follows:

$$G_{\rm VV} = \left|\frac{\dot{V}_{\rm out}}{\dot{V}_{\rm in}}\right| = \left|\frac{Z_2R_{\rm T}}{Z_1Z_2+Z_1Z_3+Z_2Z_3+(Z_1+Z_2)\,R_{\rm T}}\right|. \quad (6)$$

The input impedance $Z_{\rm in}$ of the T-circuit can be yielded as follows:

$$Z_{\rm in} = \frac{\dot{V}_{\rm in}}{\dot{I}_{\rm in}} = \frac{Z_1Z_2+Z_1Z_3+Z_2Z_3+(Z_1+Z_2)\,R_{\rm T}}{Z_2+Z_3+R_{\rm T}}. \quad (7)$$

In reference to (5) and (6), each of Z_1, Z_2, and Z_3 can be treated as a variable parameter to achieve load-independent output current and voltage. Thus, they are divided into three following scenarios to discuss.

1) Variable Parameter Z_1: In this part, Z_1 is treated as a variable.

CC output: According to (5), the transfer admittance $G_{\rm VI}$ can be load-independent when it satisfies (8)

$$(Z_1+Z_2)\,R_{\rm T} = 0. \quad (8)$$

By solving (8), we can obtain

$$Z_1 = -Z_2 = -jX_2 \quad (9)$$

Substituting (1) and (9) into (5), a new transfer admittance noted as $G_{{\rm VIZ}_1}$ is given by

$$G_{{\rm VIZ}_1} = \left|\frac{-1}{Z_2}\right| = \left|\frac{j}{X_2}\right|. \quad (10)$$

The corresponding input impedance noted as $Z_{{\rm inG_{VI}Z}_1}$ can be calculated by substituting (1) and (9) into (7), namely

$$Z_{{\rm inG_{VI}Z}_1} = \frac{X_2^2R_{\rm T}}{(X_2+X_3)^2+R_{\rm T}^2} - j\frac{(X_2+X_3)\,X_2^2}{(X_2+X_3)^2+R_{\rm T}^2} \quad (11)$$

which indicates that the input impedance $Z_{{\rm inG_{VI}Z}_1}$ with CC output can be capacitive, resistive, or inductive with different values of X_2 and X_3.

CV output: The T-circuit can have load-independent output voltage if (6) satisfies the following equation:

$$Z_1Z_2+Z_1Z_3+Z_2Z_3 = 0. \quad (12)$$

After solving (12), Z_1 can be derived as follows:

$$Z_1 = \frac{-Z_2Z_3}{Z_2+Z_3} = \frac{-jX_2X_3}{X_2+X_3}. \quad (13)$$

Thus, the new voltage gain named $G_{{\rm VVZ}_1}$ can be expressed by

$$G_{{\rm VVZ}_1} = \left|\frac{Z_2+Z_3}{Z_2}\right| = \left|\frac{X_2+X_3}{X_2}\right|. \quad (14)$$

The input impedance noted as $Z_{{\rm inG_{VV}Z}_1}$ with CV output can be rewritten as follows:

$$Z_{{\rm inG_{VV}Z}_1} = \frac{X_2^2R_{\rm T}}{(X_2+X_3)^2+R_{\rm T}^2} + j\frac{X_2^2R_{\rm T}^2}{(X_2+X_3)\left[(X_2+X_3)^2+R_{\rm T}^2\right]}. \quad (15)$$

It suggests that the input impedance $Z_{{\rm inG_{VV}Z}_1}$ might be inductive or capacitive depending on the values of X_2 and X_3.

2) Variable Parameter Z_2: In this part, Z_2 is regarded as a variable parameter.

CC output: By solving (8), we can get

$$Z_2 = -Z_1 = -jX_1. \quad (16)$$

Substituting (16) into (5), a new transfer admittance $G_{{\rm VIZ}_2}$ turns out to be

$$G_{{\rm VIZ}_2} = \left|\frac{1}{Z_1}\right| = \left|\frac{-j}{X_1}\right|. \quad (17)$$

The input impedance $Z_{{\rm inG_{VI}Z}_2}$ is shown as follows:

$$Z_{{\rm inG_{VI}Z}_2} = \frac{X_1^2R_{\rm T}}{(X_1-X_3)^2+R_{\rm T}^2} + j\frac{X_1^2\,(X_1-X_3)}{(X_1-X_3)^2+R_{\rm T}^2}. \quad (18)$$

It is evident that the input impedance $Z_{{\rm inG_{VI}Z}_2}$ could be inductive, capacitive, or resistive counting on the values of X_1 and X_3.

CV output: Similarly, by solving (12), Z_2 can be derived as follows:

$$Z_2 = \frac{-Z_1Z_3}{Z_1+Z_3} = \frac{-jX_1X_3}{X_1+X_3}. \quad (19)$$

By substituting (19) into (6), a new voltage gain named $G_{{\rm VVZ}_2}$ can be obtained as follows:

$$G_{{\rm VVZ}_2} = \left|\frac{-Z_3}{Z_1}\right| = \left|\frac{-X_3}{X_1}\right|. \quad (20)$$

The input impedance $Z_{{\rm inG_{VV}Z}_2}$ is given by

$$Z_{{\rm inG_{VV}Z}_2} = \frac{X_1^2X_3^2R_{\rm T}}{(X_1+X_3)^2R_{\rm T}^2+X_3^4} + j\frac{X_1^2\,(X_1+X_3)\,R_{\rm T}^2}{(X_1+X_3)^2R_{\rm T}^2+X_3^4} \quad (21)$$

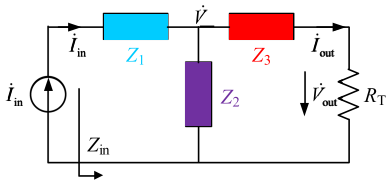

Fig. 2. T-circuit driven by a current source.

which also could be inductive, capacitive, or resistive with different values of X_1 and X_3.

3) Variable Parameter Z_3: In this part, Z_3 is considered as a variable. On the basis of (5) and (8), no matter what the value of Z_3 is, it is impossible for the T-circuit to have CC output. Therefore, this condition, when Z_3 is a variable parameter, is impractical. Besides, there is no need for discussing CV output.

B. Analysis of a T-Circuit Driven by a Current Source

Fig. 2 illustrates a T-circuit driven by a sinusoidal current source with angular frequency ω. Since Z_1 is connected with the current source, Z_1 only can affect the input impedance Z_{in} and has nothing to do with the output current I_{out} and voltage V_{out}. Z_1 should not be regarded as a variable parameter.

According to Kirchhoff's current law, the T-circuit can be described by

$$\dot{I}_{\text{in}} = \dot{V}\left(\frac{1}{Z_2} + \frac{1}{Z_3 + R_{\text{T}}}\right). \tag{22}$$

Afterward, the output current $\dot{I}_{\text{out}}$ and the output voltage $\dot{V}_{\text{out}}$ can be attained as follows:

$$\dot{I}_{\text{out}} = \frac{Z_2\dot{I}_{\text{in}}}{Z_2 + Z_3 + R_{\text{T}}}, \quad \dot{V}_{\text{out}} = \frac{Z_2 R_{\text{T}}\dot{I}_{\text{in}}}{Z_2 + Z_3 + R_{\text{T}}}. \tag{23}$$

Hence, the current gain G_{II}, defined as the ratio of the output current $\dot{I}_{\text{out}}$ to the input current $\dot{I}_{\text{in}}$, can be obtained as follows:

$$G_{\text{II}} = \left|\frac{\dot{I}_{\text{out}}}{\dot{I}_{\text{in}}}\right| = \left|\frac{Z_2}{Z_2 + Z_3 + R_{\text{T}}}\right|. \tag{24}$$

Similarly, the transfer impedance G_{IV}, the ratio between the output voltage $\dot{V}_{\text{out}}$ and the input current $\dot{I}_{\text{in}}$, is expressed as follows:

$$G_{\text{IV}} = \left|\frac{\dot{V}_{\text{out}}}{\dot{I}_{\text{in}}}\right| = \left|\frac{Z_2 R_{\text{T}}}{Z_2 + Z_3 + R_{\text{T}}}\right|. \tag{25}$$

The input impedance Z_{in} is the same as (7) because the components are the same in the T-circuit.

In view of (25) and (24), Z_2 and Z_3 can be treated as a variable parameter, so two categories should be analyzed.

1) Variable Parameter Z_2: In this part, Z_2 is considered as a variable parameter.

CC output: In accordance with (24), to let the T-circuit have CC output, the only way is to set Z_2 equal to ∞. Thus, the new current gain noted as G_{IIZ_2} is yielded as follows:

$$G_{\text{IIZ}_2} = \left|\lim_{Z_2\to\infty}\frac{Z_2}{Z_2 + Z_3 + R_{\text{T}}}\right| = 1. \tag{26}$$

The input impedance Z_{in} in (7) can be rewritten as follows:

$$\begin{aligned} Z_{\text{in}G_{\text{II}}Z_2} &= \lim_{Z_2\to\infty}\frac{Z_1Z_2 + Z_1Z_3 + Z_2Z_3 + (Z_1 + Z_2)R_{\text{T}}}{Z_2 + Z_3 + R_{\text{T}}} \\ &= R_{\text{T}} + j(X_1 + X_3) \end{aligned} \tag{27}$$

which can be inductive, capacitive, or resistive in terms of the values of X_1 and X_3.

CV output: In order to realize CV output, (25) should satisfy (28)

$$Z_2 + Z_3 = 0. \tag{28}$$

By solving (28), we can get

$$Z_2 = -Z_3 = -jX_3. \tag{29}$$

Then, the new transfer impedance noted as G_{IVZ_2} can be acquired by substituting (29) into (25), i.e.

$$G_{\text{IVZ}_2} = |-Z_3| = |-jX_3|. \tag{30}$$

Substituting (29) into (7), the new input impedance named $Z_{\text{in}G_{\text{IV}}Z_2}$ is shown as follows:

$$Z_{\text{in}G_{\text{IV}}Z_2} = \frac{X_3^2}{R_{\text{T}}} + j(X_1 - X_3). \tag{31}$$

It hints that the input impedance also might be inductive, capacitive, or resistive relying on the values of X_1 and X_3.

2) Variable Parameter Z_3: In this part, Z_3 is regarded as a variable parameter. According to (24), it is impossible for the T-circuit to have CC output whatever the value of Z_3 is. Consequently, this circumstance, when Z_3 is a variable parameter, is meaningless to discuss, as well as CV output.

As a result, a T-circuit driven by a voltage or current source can achieve CC and CV outputs with variable parameters. All the possible cases are listed in Table I, from which some conclusions can be drawn as follows.

1) The VT can transfer CV input to CC or CV output by altering the value of one variable parameter. Besides, CC input can also be transferred to CC or CV output.
2) The input impedance of VT with CC and CV outputs has three possible situations:
   a) one is inductive and the other one is capacitive;
   b) both are inductive or capacitive;
   c) one is resistive and the other one is inductive or capacitive.

Based on these conclusions, we can employ the VT for an IPT charging system. For applications with different requirements, corresponding VTs can be chosen.

III. IPT System Using VT for Battery Charging

A. Analysis of CC and CV Outputs

All the cases given in Table I can be used for IPT systems with different requirements. A VT can be placed on the secondary side to cancel the wireless communication link. In this paper, aiming at a compact and light secondary side, a VT is selected to put on the primary side. Besides, since the input of the compensation topology is usually square wave voltage, CASE II (T-circuit with

TABLE I
T-CIRCUIT WITH DIFFERENT VARIABLE PARAMETERS

	CASE I Variable Z_1 (voltage source)			CASE II Variable Z_2 (voltage source)			CASE III Variable Z_2 (current source)		
Variable Parameter	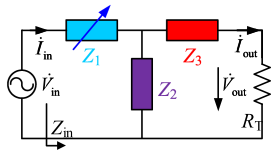			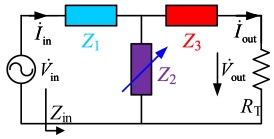			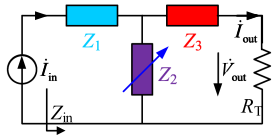		
CC Output	$G_{\mathrm{VIZ_1}}=\lvert j/X_2\rvert$ $(Z_1=-jX_2)$			$G_{\mathrm{VIZ_2}}=\lvert -j/X_1\rvert$ $(Z_2=-jX_1)$			$G_{\mathrm{IIZ_2}}=1$ $(Z_2\to\infty)$		
Input impedance	$Z_{\mathrm{inG_{VI}Z_1}}=X_2^2R_\mathrm{T}/\left[(X_2+X_3)^2+R_\mathrm{T}^2\right]$ $-j(X_2+X_3)X_2^2/\left[(X_2+X_3)^2+R_\mathrm{T}^2\right]$			$Z_{\mathrm{inG_{VI}Z_2}}=X_1^2R_\mathrm{T}/\left[(X_1-X_3)^2+R_\mathrm{T}^2\right]$ $+jX_1^2(X_1-X_3)/\left[(X_1-X_3)^2+R_\mathrm{T}^2\right]$			$Z_{\mathrm{inG_{II}Z_2}}=R_\mathrm{T}+j(X_1+X_3)$		
	$X_2+X_3>0$	$X_2+X_3=0$	$X_2+X_3<0$	$X_1-X_3>0$	$X_1-X_3=0$	$X_1-X_3<0$	$X_1+X_3>0$	$X_1+X_3=0$	$X_1+X_3<0$
	capacitive	resistive	inductive	inductive	resistive	capacitive	inductive	resistive	capacitive
CV Output	$G_{\mathrm{VVZ_1}}=\lvert(X_2+X_3)/X_2\rvert$ $(Z_1=-jX_2X_3/(X_2+X_3))$			$G_{\mathrm{VVZ_2}}=\lvert -X_3/X_1\rvert$ $(Z_2=-jX_1X_3/(X_1+X_3))$			$G_{\mathrm{IVZ_2}}=\lvert -jX_3\rvert$ $(Z_2=-jX_3)$		
Input impedance	$Z_{\mathrm{inG_{VV}Z_1}}=X_2^2R_\mathrm{T}/\left[(X_2+X_3)^2+R_\mathrm{T}^2\right]$ $+jX_2^2R_\mathrm{T}^2/\left\{(X_2+X_3)\left[(X_2+X_3)^2+R_\mathrm{T}^2\right]\right\}$			$Z_{\mathrm{inG_{VV}Z_2}}=X_1^2X_3^2R_\mathrm{T}/\left[(X_1+X_3)^2R_\mathrm{T}^2+X_3^4\right]$ $+jX_1^2(X_1+X_3)R_\mathrm{T}^2/\left[(X_1+X_3)^2R_\mathrm{T}^2+X_3^4\right]$			$Z_{\mathrm{inG_{IV}Z_2}}=X_3^2/R_\mathrm{T}+j(X_1-X_3)$		
	$X_2+X_3>0$	$X_2+X_3=0$	$X_2+X_3<0$	$X_1+X_3>0$	$X_1+X_3=0$	$X_1+X_3>0$	$X_1-X_3>0$	$X_1-X_3=0$	$X_1-X_3<0$
	inductive	impossible	capacitive	inductive	resistive	capacitive	inductive	resistive	capacitive

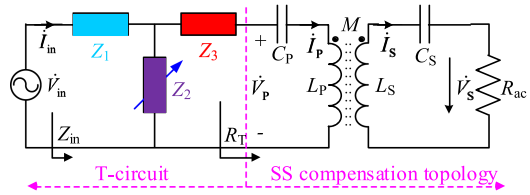

Fig. 3. T-circuit cascaded with an SS compensation topology.

variable parameter Z_2 driven by a voltage source) is chosen for an IPT charging system. A VT cascaded with an SS compensation topology (VTSS) is illustrated in Fig. 3. L_P, L_S, and M are the primary side coil inductance, secondary side coil inductance, and mutual inductance, respectively. R_ac is the equivalent ac load. C_P and C_S are utilized to compensate the inductances of the primary and secondary coils L_P and L_S, i.e.

$$\begin{cases} C_\mathrm{P}=1/\left(\omega^2L_\mathrm{P}\right) \\ C_\mathrm{S}=1/\left(\omega^2L_\mathrm{S}\right). \end{cases} \tag{32}$$

According to KVL, the SS compensation topology can be described by

$$\begin{bmatrix} \dot{V}_\mathrm{P} \\ 0 \end{bmatrix}=\begin{bmatrix} \frac{1}{j\omega C_\mathrm{P}}+j\omega L_\mathrm{P} & -j\omega M \\ -j\omega M & \frac{1}{j\omega C_\mathrm{S}}+j\omega L_\mathrm{S}+R_\mathrm{ac} \end{bmatrix}\begin{bmatrix} \dot{I}_\mathrm{P} \\ \dot{I}_\mathrm{S} \end{bmatrix}. \tag{33}$$

Solving (33) by substituting (32) into (33), the primary and secondary coil currents are derived as follows:

$$\dot{I}_\mathrm{P}=\frac{R_\mathrm{ac}\dot{V}_\mathrm{P}}{\omega^2M^2},\quad \dot{I}_\mathrm{S}=\frac{j\dot{V}_\mathrm{P}}{\omega M}. \tag{34}$$

Afterward, the voltage of R_ac is given by

$$\dot{V}_\mathrm{S}=\frac{jR_\mathrm{ac}\dot{V}_\mathrm{P}}{\omega M}. \tag{35}$$

The transfer admittance G_VISS of SS topology can be yielded as follows:

$$G_\mathrm{VISS}=\left|\frac{\dot{I}_\mathrm{S}}{\dot{V}_\mathrm{S}}\right|=\left|\frac{1}{j\omega M}\right|. \tag{36}$$

Likewise, the transfer impedance G_IVSS of SS topology is obtained as follows:

$$G_\mathrm{IVSS}=\left|\frac{\dot{V}_\mathrm{S}}{\dot{I}_\mathrm{P}}\right|=\left|j\omega M\right|. \tag{37}$$

It is evident that the SS compensation topology can transfer CV (or CC) input to CC (or CV) output, which indicates that the SS topology is a special case of T-circuit.

The input impedance R_T of SS topology can be attained as follows:

$$R_\mathrm{T}=\frac{\dot{V}_\mathrm{P}}{\dot{I}_\mathrm{P}}=\frac{\omega^2M^2}{R_\mathrm{ac}} \tag{38}$$

which can be resistive if the equivalent ac load R_ac is a resistance load.

On the basis of the analysis for CASE II, the transfer admittance $G_\mathrm{VI\text{-}VTSS}$ of the proposed VTSS can be expressed by

$$G_\mathrm{VI\text{-}VTSS}=\left|\frac{\dot{I}_\mathrm{S}}{\dot{V}_\mathrm{in}}\right|=G_{\mathrm{VVZ_2}}\times G_\mathrm{VISS}=\left|\frac{-jX_3}{X_1\omega M}\right|. \tag{39}$$

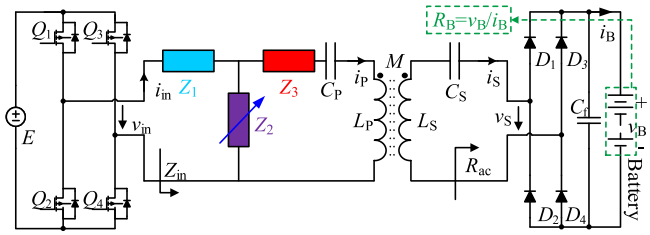

Fig. 4. Diagram of an IPT system with VTSS for battery charging.

In the same way, the voltage gain $G_{\text{VV-VTSS}}$ of the VTSS is obtained as follows:

$$G_{\text{VV-VTSS}} = \left|\frac{\dot{V}_S}{\dot{V}_{in}}\right| = G_{\text{VIZ}_2} \times G_{\text{IVSS}} = \left|\frac{\omega M}{X_1}\right|. \tag{40}$$

B. Parameter Design for VTSS

According to CASE II, if the input impedance of VT with CC and CV outputs are required to be resistive, the parameters of T-circuit should satisfy

$$X_1 - X_3 = 0 \ \text{ or } X_1 + X_3 = 0. \tag{41}$$

Substituting (41) into (39), we can find that the transfer admittance of proposed VTSS is simplified as follows:

$$G_{\text{VI-VTSS}} = \left|\frac{-jX_3}{X_1\omega M}\right| = \left|\pm\frac{j}{\omega M}\right|. \tag{42}$$

The output current is only related to the mutual inductance M, i.e., once the parameters of LCT are fixed, the output current of VTSS is hard to alter unless using another LCT with a new mutual inductance. Therefore, in order to let the output voltage/current have design freedom with the constraints of LCT parameters, it is better to make the input impedance of VT with CC and CV outputs both inductive. In that way, the output current and voltage can be changed by tuning the parameters (X_1 and X_3) of VT without using another new LCT.

An IPT system with VTSS for battery charging is shown in Fig. 4, where E, I_B, and V_B are the input dc voltage, charge current in CC mode, and charge voltage in CV mode, respectively. According to [26], the output voltage V_{in} of the inverter, output current I_B, and output voltage V_B of the rectifier can be expressed by

$$V_{in} = \frac{2\sqrt{2}E}{\pi}, \quad V_B = \frac{\pi\sqrt{2}}{4}V_S, \quad I_B = \frac{2\sqrt{2}}{\pi}I_S. \tag{43}$$

The relationship between the equivalent ac load R_{ac} and battery equivalent load R_B can be given by [9]

$$R_{ac} = \frac{8}{\pi_2}R_B. \tag{44}$$

Substituting (43) into (40), the value of X_1 is yielded as follows:

$$X_1 = \pm\frac{\omega EM}{V_B}. \tag{45}$$

Similarly, the value of X_3 can be calculated by substituting (43) into (39), i.e.

$$X_3 = \pm\frac{\pi^2 I_B \omega^2 M^2}{8V_B}. \tag{46}$$

Then, the value of X_2 in VTSS for CC output can be attained by substituting (45) and (46) into (19), namely

$$X_{2CC} = \pm\frac{\pi^2 I_B E\omega^2 M^2}{8V_B E + \pi^2\omega M V_B I_B}. \tag{47}$$

Substituting (45) and (46) into (16), the value of X_2 in VTSS for CV output is obtained as follows:

$$X_{2CV} = \pm\frac{\omega ME}{V_B}. \tag{48}$$

All the values of E, M, I_B, and V_B are positive, while the values of $X_1 - X_3$ can be positive or negative in terms of (45)–(48). If the values of $X_1 - X_3$ are positive, the components $Z_1 - Z_3$ should be inductors. Otherwise, they are capacitors if the values of $X_1 - X_3$ are negative. The detailed values of all the parameters in T-circuit, all possible combinations of inductors and capacitors, input impedance angle are listed in Table II.

From Table II, we can find that the input impedance of T(c) in CC mode is capacitive, and the input impedance of T(d) in CV mode is also capacitive. Thus, T(c) and T(d) should not be employed for VTSS with the requirement of zero voltage switching. As for T(a) and T(b), the input impedance of theirs both are inductive. It is distinct that the input impedance angle of T(a) in CC mode is larger than that in CV mode, but that of T(b) is opposite. The more inductive the input impedance is, the more reactive power is in the IPT system. Too much reactive power can cause a large power loss in the IPT system. Additionally, the charging time in CV mode is longer than that in CC mode for a lead acid battery [23]. Therefore, to reduce the power loss caused by reactive power in the whole charging process, T(a) is applied to VTSS in this paper. Also, other VTs can be employed for different applications according to various requirements. For instance, T(b) can be selected to use for lithium-ion battery charging, where the charging time in CC mode is shorter than that in CV mode.

In T(a), the values of X_2 in CC and CV mode are different. Thus, an ac switch S is used to alter the value of parameter X_2, namely, to switch the charging mode from CC mode to CV mode, as shown in Fig. 5. There are two possible ways to alter the parameter.

1) In Fig. 5(a), when the switch S is OFF, the IPT system with VTSS is in CV mode. We have

$$\frac{1}{j\omega C_{2CV}} = jX_{2CV} = -\frac{j\omega EM}{V_B}. \tag{49}$$

After solving (49), the value of capacitor C_{2CC} is given by

$$C_{2CV} = \frac{V_B}{EM\omega^2}. \tag{50}$$

When the switch S is ON, it is in CC mode, and we have

$$\frac{1}{j\omega\left(C_{2CCP} + C_{2CV}\right)} = jX_{2CC} = -j\frac{\pi^2 I_B E\omega^2 M^2}{8V_B E + \pi^2\omega M V_B I_B}. \tag{51}$$

TABLE II
VALUES OF PARAMETERS IN T-CIRCUIT

Parameter	T(a)	T(b)	T(c)	T(d)
X_1	$\omega EM / V_B$	$\omega EM / V_B$	$-\omega EM / V_B$	$-\omega EM / V_B$
X_3	$\pi^2 I_B \omega^2 M^2 / (8V_B)$	$-\pi^2 I_B \omega^2 M^2 / (8V_B)$	$\pi^2 I_B \omega^2 M^2 / (8V_B)$	$-\pi^2 I_B \omega^2 M^2 / (8V_B)$
X_{2CC}	$-\frac{\pi^2 I_B E \omega^2 M^2}{8V_B E + \pi^2 \omega M V_B I_B}$	$\frac{\pi^2 I_B E \omega^2 M^2}{8V_B E + \pi^2 \omega M V_B I_B}$	$\frac{\pi^2 I_B E \omega^2 M^2}{8V_B E - \pi^2 \omega M V_B I_B}$	$\frac{\pi^2 I_B E \omega^2 M^2}{8V_B E + \pi^2 \omega M V_B I_B}$
Input impedance angle (CC)	$\arctan\left(\frac{8V_B E + \pi^2 \omega M V_B I_B}{\pi^2 \omega M R_B I_B^2}\right)$	$\arctan\left(\frac{8V_B E - \pi^2 \omega M V_B I_B}{\pi^2 \omega M R_B I_B^2}\right)$	$\arctan\left(-\frac{8V_B E + \pi^2 \omega M V_B I_B}{\pi^2 \omega M R_B I_B^2}\right)$	$\arctan\left(-\frac{8V_B E - \pi^2 \omega M V_B I_B}{\pi^2 \omega M R_B I_B^2}\right)$
X_{2CV}	$-\omega EM / V_B$	$-\omega EM / V_B$	$\omega EM / V_B$	$\omega EM / V_B$
Input impedance angle (CV)	$\arctan\left(\frac{8R_B E - \pi^2 \omega M R_B I_B}{\pi^2 \omega M V_B}\right)$	$\arctan\left(\frac{8R_B E + \pi^2 \omega M R_B I_B}{\pi^2 \omega M V_B}\right)$	$\arctan\left(-\frac{8R_B E - \pi^2 \omega M R_B I_B}{\pi^2 \omega M V_B}\right)$	$\arctan\left(-\frac{8R_B E + \pi^2 \omega M R_B I_B}{\pi^2 \omega M V_B}\right)$
T-Circuit	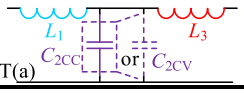	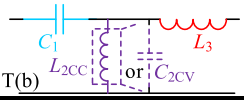	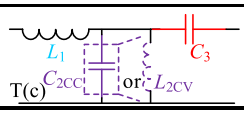	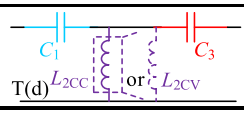

where if $X_1 > 0$, $jX_1 = j\omega L_1$; $X_1 < 0$, $jX_1 = 1/(j\omega C_1)$; $X_3 > 0$, $jX_3 = j\omega L_3$; $X_3 < 0$, $jX_3 = 1/(j\omega C_3)$; $X_{2CC} > 0$, $jX_{2CC} = j\omega L_{2CC}$; $X_{2CC} < 0$, $jX_{2CC} = 1/(j\omega C_{2CC})$; $X_{2CV} > 0$, $jX_{2CV} = j\omega L_{2CV}$; $X_{2CV} < 0$, $jX_{2CV} = 1/(j\omega C_{2CV})$.

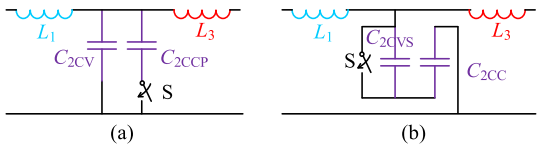

Fig. 5. Two ways for altering variable parameter (a) in parallel and (b) in series.

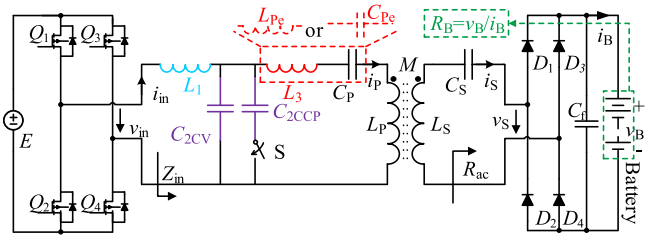

Fig. 6. Proposed IPT system for battery charging.

Thus, the value of capacitor C_{2CCP} can be derived as follows:

$$C_{2CCP} = \frac{8V_B}{\pi^2 I_B \omega^3 M^2}. \tag{52}$$

2) In Fig. 5(b), when the switch S is ON, the IPT system is in CC mode, i.e.

$$\frac{1}{j\omega C_{2CC}} = jX_{2CC} = -j\frac{\pi^2 I_B E \omega^2 M^2}{8V_B E + \pi^2 \omega M V_B I_B}. \tag{53}$$

After solving (53), the capacitor C_{2CC} is yielded as follows:

$$C_{2CC} = \frac{8V_B E + \pi^2 \omega M V_B I_B}{\pi^2 I_B E \omega^3 M^2}. \tag{54}$$

When the switch S is OFF, it is in CV mode, so we have

$$\frac{1}{j\omega C_{2CC}} + \frac{1}{j\omega C_{2CVS}} = jX_{2CV} = -\frac{j\omega EM}{V_B}. \tag{55}$$

Then, the capacitor C_{2CVS} can be expressed by

$$C_{2CVS} = \frac{V_B\left(8E + \pi^2 \omega I_B M\right)}{8M\omega^2 E^2}. \tag{56}$$

For simplification, the way of parallel connection is selected in the experiment for verification, as shown in Fig. 6. Inductors L_1 and L_3 are given by

$$L_1 = \frac{EM}{V_B}, \quad L_3 = \frac{\pi^2 \omega I_B M^2}{8V_B}. \tag{57}$$

In practice, inductor L_3 and capacitor C_P can be treated as one component, which may be an inductor L_{Pe} or a capacitor C_{Pe}, i.e.

$$\begin{cases} L_{Pe} = \frac{\pi^2 \omega I_B M^2 - 8V_B L_P}{8V_B}, & j\omega L_3 + \frac{1}{j\omega C_P} > 0 \\ C_{Pe} = \frac{8V_B}{\omega^2(8V_B L_P - \pi^2 \omega I_B M^2)}, & j\omega L_3 + \frac{1}{j\omega C_P} < 0. \end{cases} \tag{58}$$

Finally, the parameters of the IPT system with VTSS can be obtained regarding (32), (50), (52), (57), and (58).

When the switch S is ON, the system operates in the CC mode. The current i_{PCC} in the primary coil can be calculated as follows:

$$i_{PCC} = \frac{2\sqrt{2}I_B}{\pi\omega M} R_B \tag{59}$$

which indicates that the current i_{PCC} will increase with the rise of the battery equivalent load R_B in CC mode. When the switch S is OFF, the system runs in CV mode. The current i_{PCV} in the primary coil can be given as follows:

$$i_{PCV} = \frac{2\sqrt{2}V_B}{\pi\omega M} \tag{60}$$

which demonstrates that the primary coil current i_{PCV} is constant in the CV mode. When the charging mode changes from CC to CV, the battery equivalent load noted as R_{B0} can be given as $R_{B0} = V_B / I_B$. At this moment, the current in the primary coil is calculated as follows:

$$i_{PCC0} = \frac{2\sqrt{2}I_B}{\pi\omega M} R_{B0} = \frac{2\sqrt{2}I_B}{\pi\omega M} \cdot \frac{V_B}{I_B} = \frac{2\sqrt{2}V_B}{\pi\omega M}. \tag{61}$$

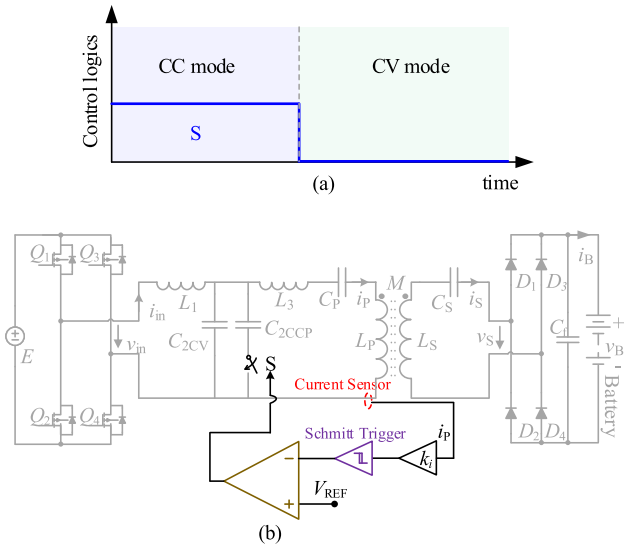

Fig. 7. (a) Control logic for S, and (b) control diagram of the proposed IPT charger without communication, where $k_i = V_{\mathrm{REF}}/i_{\mathrm{PCV}}$.

It is obvious that current i_{PCC0} equals to the current i_{PCV} in the CV mode. Therefore, the value of the current in the primary coil can be measured for the switch of charging mode so the wireless communication link is not required. The control logic of the ac switch S is depicted in Fig. 7(a), and the control diagram of the charging mode is detailed in Fig. 7(b). A current sensor is used to measure the primary coil current i_{P}. The proposed IPT system operates in CC mode when $i_{\mathrm{P}} < i_{\mathrm{PCV}}$. Once i_{P} hits the value of i_{PCV}, switch S is triggered, and the system goes into the CV mode. It should be noted that this technique only can be used when the M and ω are fixed.

It should accentuate that the proposed method aims at applications with very small or no misalignment, such as electric bicycles charging [5], [24]. However, if the method is used in some other applications that indeed face misalignments, some commercial ICs like UCC3895 can be adopted to implement fixed-frequency duty cycle control for the system to maintain outputs stable [19]. In this circumstance, the output voltage V_{in} of the inverter in (43) should be rewritten as follows:

$$V_{\mathrm{in}} = \frac{2\sqrt{2}E}{\pi}\sin\left(\frac{\pi D}{2}\right) \tag{62}$$

where D is the duty cycle of V_{in} of the fixed-frequency duty cycle control. Then, the other parameters can be calculated according to the aforementioned equations.

Additionally, the previous control diagram of the proposed approach is no longer applicable since mutual inductance M is not fixed. The charging voltage v_{B} is used for the switch of charging mode, and the switching control signals are delivered through a wireless communication link [24], as depicted in Fig. 8. A voltage sensor is used to measure the charging voltage v_{B}. The proposed IPT system operates in CC mode when $v_{\mathrm{B}} < V_{\mathrm{B}}$. Once v_{B} reaches the charge voltage V_{B}, switch S is triggered, and the system goes into the CV mode.

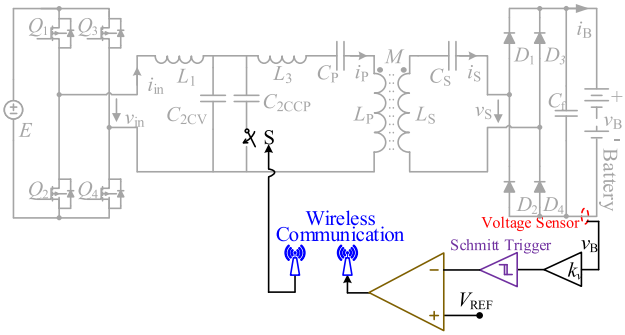

Fig. 8. Control diagram of the proposed IPT charger with communication, where $k_v = V_{\mathrm{REF}}/V_{\mathrm{B}}$ and V_{REF} are the voltage ratio and the reference voltage, respectively.

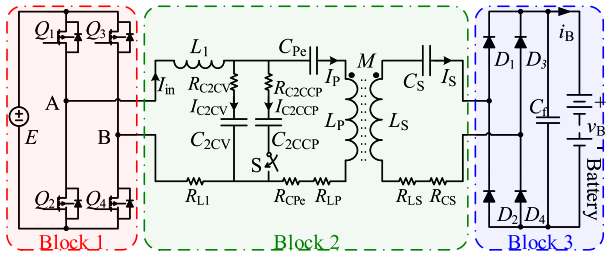

Fig. 9. IPT system divided into three blocks.

C. Analysis of Power Losses

In this part, inductor L_3 and capacitor C_{P} is treated as a capacitor C_{Pe} for simplification. The equivalent series resistance (ESR) of each component is taken into consideration. The proposed IPT system from dc input to dc output is predominantly divided into three parts: a high-frequency inverter, a magnetic coupler with compensation topology, and a full-bridge rectifier, as shown in Fig. 9.

1) Power Losses of Block 1: The power losses of the high-frequency inverter comprise the conduction loss $P_{\mathrm{cond\_MOS}}$ of the MOSFETs, the conduction loss $P_{\mathrm{cond\_D}}$ of the body diodes, and the switching loss $P_{\mathrm{SW\_MOS\_D}}$ of the MOSFETs and the diodes. $P_{\mathrm{cond\_MOS}}$ and $P_{\mathrm{cond\_D}}$ are given by [27]

$$\begin{cases} P_{\mathrm{cond\_MOS}} = \frac{1}{\pi} r_{\mathrm{DS}} I_{\mathrm{in}}^2 \left(\pi + \varphi + \sin\varphi\right) \\ P_{\mathrm{cond\_D}} = \frac{2\sqrt{2}}{\pi} V_{\mathrm{f}} I_{\mathrm{in}} \left(1 - \sin\frac{\varphi}{2}\right) + \frac{1}{\pi} r_{\mathrm{D}} I_{\mathrm{in}}^2 \left(\pi - \varphi - \sin\varphi\right) \end{cases} \tag{63}$$

where r_{DS}, I_{in}, φ, V_{f}, and r_{D} are the drain–source on-state resistance of the MOSFET, the output current of the inverter, the conduction angle of the inverter, the threshold voltage and equivalent on-state resistance of the body diode, respectively. $P_{\mathrm{SW\_MOS\_D}}$ is expressed by [27]

$$P_{\mathrm{SW\_MOS\_D}} = 2EI_{\mathrm{in}}\sqrt{2}\cos\left(\frac{\varphi}{2}\right) \times f\left(\frac{e_{\mathrm{SW\_ON}} + e_{\mathrm{SW\_OFF}}}{V_{\mathrm{R}} I_{\mathrm{R}}} + \frac{Q_{\mathrm{RR}}}{I_{\mathrm{R\_D}}}\right) \tag{64}$$

where $e_{\mathrm{SW\_ON}}$ and $e_{\mathrm{SW\_OFF}}$ are the turn-ON and turn-OFF energy losses of the MOSFET; V_{R} and I_{R} are the drain–source voltage and source current of the MOSFET; Q_{RR} and $I_{\mathrm{R\_D}}$ are reverse recovery charge and the reference current of the diode, respectively. Therefore, the power losses of Block 1 is obtained as follows:

$$P_{\mathrm{loss\_1}} = P_{\mathrm{cond\_MOS}} + P_{\mathrm{cond\_D}} + P_{\mathrm{SW\_MOS\_D}}. \tag{65}$$

2) Power Losses of Block 2: The ESR of each component of Block 2 can be measured by an *LCR* meter. The power loss of each component (inductor or capacitor) can be calculated by

$$P_{\mathrm{RX}} = R_{\mathrm{X}} I_{\mathrm{X}}^2 \tag{66}$$

where R_{X} is the ESR of the inductor or capacitor, and I_{X} is the rms value of the current flowing through the corresponding component. When the ac switch S is connected in the circuit, the power loss of S should be considered. Since switch S only turns ON or turns OFF for once, the conduction loss is inevitable, and switching loss can be ignored. The ac switch consists of two anti-series connected MOSFETs. Hence, the power loss $P_{\mathrm{loss\_S}}$ of the ac switch S can be given by

$$P_{\mathrm{loss\_S}} = 2 r_{\mathrm{DSS}} I_{\mathrm{C2CCP}}^2 \tag{67}$$

where r_{DSS} is the drain–source on-state resistance of the MOSFET.

In the CC mode, the switch S is ON. The power losses $P_{\mathrm{loss_}}$2CC of the Block 2 is expressed by

$$\begin{aligned} P_{\mathrm{loss\_2CC}} = {} & I_{\mathrm{in}}^2 R_{\mathrm{L1}} + I_{\mathrm{C2CV}}^2 R_{\mathrm{C2CV}} + I_{\mathrm{C2CCP}}^2 R_{\mathrm{C2CCP}} \\ & + P_{\mathrm{loss\_S}} + I_{\mathrm{P}}^2 \left(R_{\mathrm{CPe}} + R_{\mathrm{LP}}\right) + I_{\mathrm{S}}^2 \left(R_{\mathrm{CS}} + R_{\mathrm{LS}}\right). \end{aligned} \tag{68}$$

In the CV mode, the switch S is OFF. The power losses $P_{\mathrm{loss\_2CV}}$ of the Block 2 is given by

$$\begin{aligned} P_{\mathrm{loss\_2CV}} = {} & I_{\mathrm{in}}^2 R_{\mathrm{L1}} + I_{\mathrm{C2CV}}^2 R_{\mathrm{C2CV}} \\ & + I_{\mathrm{P}}^2 \left(R_{\mathrm{CPe}} + R_{\mathrm{LP}}\right) + I_{\mathrm{S}}^2 \left(R_{\mathrm{CS}} + R_{\mathrm{LS}}\right). \end{aligned} \tag{69}$$

3) Power Losses of Block 3: The power losses of the full bridge rectifier are mainly caused by the forward voltage drop of the rectifier diodes. According to [28], the power losses can be given by

$$P_{\mathrm{loss\_3}} = \frac{2\sqrt{2}}{\pi} V_{\mathrm{F}} I_{\mathrm{S}} + r_{\mathrm{CF}} I_{\mathrm{S}}^2 \tag{70}$$

where V_{F} and r_{CF} are the threshold voltage and the equivalent ON-state resistance of the diodes in the rectifier.

Finally, the total power losses P_{loss} of the IPT system are expressed by

$$\begin{cases} P_{\mathrm{loss}} = P_{\mathrm{loss\_1}} + P_{\mathrm{loss\_2CC}} + P_{\mathrm{loss\_3}}, & \text{in CC mode} \\ P_{\mathrm{loss}} = P_{\mathrm{loss\_1}} + P_{\mathrm{loss\_2CV}} + P_{\mathrm{loss\_3}}, & \text{in CV mode.} \end{cases} \tag{71}$$

D. Differences Between This Work and [20]

In order to show the differences between the proposed method and that in [20], comparisons between these two methods are elaborated as follows.

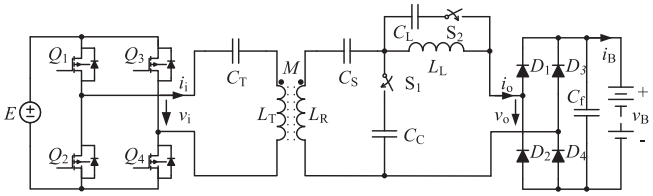

Fig. 10. System diagram of the method used in [20].

1) This Work: The proposed approach is depicted in Fig. 6.

In CC mode (S is ON): The capacitors C_{2CV} and C_{2CCP} are connected in parallel, and they can be regarded as one capacitor. It is easy to figure out that the primary compensation topology is a T-circuit.

In CV mode (S is OFF): The capacitor C_{2CV} is connected in the circuit, and C_{2CCP} is not. It is evident that the primary compensation topology is still a T-circuit.

The ac switch is just utilized to alter the parameter value of T-circuit. Thus, the compensation topology is the same in CC and CV modes.

2) Method in [20]: The method in [20] is shown in Fig. 10.

In CC mode (S_1 is OFF, and S_2 is ON): The capacitor C_{C} is not connected in the circuit, and capacitors C_{S}, C_{L} and inductor L_{L} are treated as one capacitor. We can find out that the secondary compensation topology is series (S).

In CV mode (S_1 is ON, and S_2 is OFF): The capacitor C_{C} is connected in the circuit, and capacitor C_{L} is not. It is evident that the secondary compensation topology is LCC.

The ac switches are used to change the compensation topologies. Therefore, the compensation topology in CC mode is SS, while that in CV mode is S-LCC.

All in all, the proposed method in this paper does differ fundamentally from the approach in [20] regardless of the compensation topology placed on the primary or the secondary side. Compared with the approach in [20], the proposed IPT system owns design freedom of charge current/voltage and has a smaller number of components. Besides, wireless communication is required because the T-circuit is put on the primary side for simplifying the secondary side. Additionally, the peak efficiency of the proposed method is higher than that in [20], but the average efficiency is a little lower due to the large reactive power in CC mode.

IV. Experimental Results

A. Experimental Prototype

To verify the validity of the theoretical analyses, a prototype IPT battery charger with 4 A charge current and 100 V charge voltage was implemented using the VTSS as illustrated in Fig. 11. The air gap between the primary and secondary coils is set as 150 mm, and the two coils are symmetrical double-D pad (coil size = 400 mm × 400 mm). The MOSFETs $Q_1 - Q_4$ are C2M0080120D, and the rectifier diodes $D_1 - D_4$ are DSEI $2 \times 61 - 06$C. The MOSFETs of ac switch S are APT56F50L. The system parameters are listed in Table III. First, an electronic load (ITECH IT8816B) is used to test the output

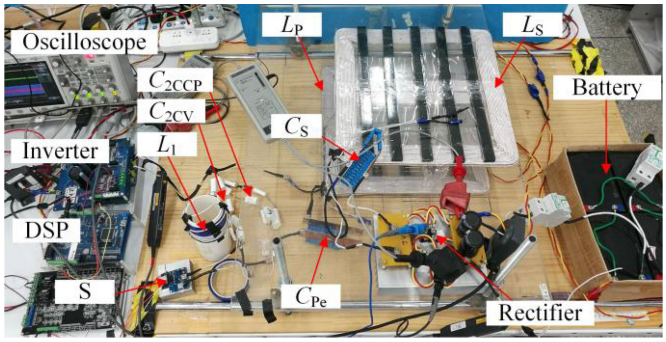

Fig. 11. Setup of the IPT battery charger.

TABLE III
SYSTEM SPECIFICATION AND PARAMETER VALUES

Parameter	value	Parameter	value
E	110 V	f	85 kHz
L_1	41.99 μH	C_{2CV}	83.50 nF
C_{2CCP}	81.30 nF	L_P	223.88 μH
M	39.72 μH	L_S	232.67 μH
C_S	15.08 nF	C_{Pe}	18.02 nF
R_{L1}	0.042 Ω	R_{C2CV}	0.016 Ω
R_{C2CCP}	0.018 Ω	R_{CPe}	0.015 Ω
R_{LP}	0.22 Ω	R_{LS}	0.20 Ω
R_{CS}	0.028 Ω	r_{DSS}	0.085 Ω
r_{DS}	0.08 Ω	φ	π
V_F	1.8 V	r_{CF}	0.0047 Ω

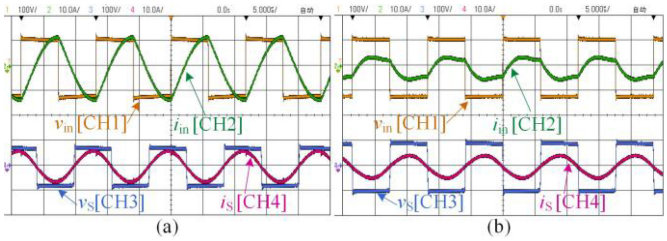

Fig. 12. Experimental waveforms of v_{in}, i_{in}, v_S, and i_S (a) at $R_B = 20\,\Omega$ in CC mode, and (b) at $R_B = 35\,\Omega$ in CV mode.

current and voltage of the proposed IPT battery charger for simplification. Then, a lead-acid battery with 48 V/12AH rating ($4 \times 6 - \mathrm{DZM} - 12$ from TIANNENG GROUP) is employed to test the charging profile of the IPT charger.

B. Experimental Results

1) Performance of the Electronic Load: Assume that the electronic load varies from 20 to 25 Ω in CC mode, while it is altered from 25 to 270 Ω in CV mode. Fig. 12 shows the experimental waveforms of output voltage/current of the inverter and input voltage/current of the rectifier. It is obvious that the input impedance angle in the CC mode is larger than that in the CV mode, which is coincident with the theoretical analysis.

The charging profile, corresponding efficiency (dc to dc), and charging power are drawn in Fig. 13. The fluctuation of charging

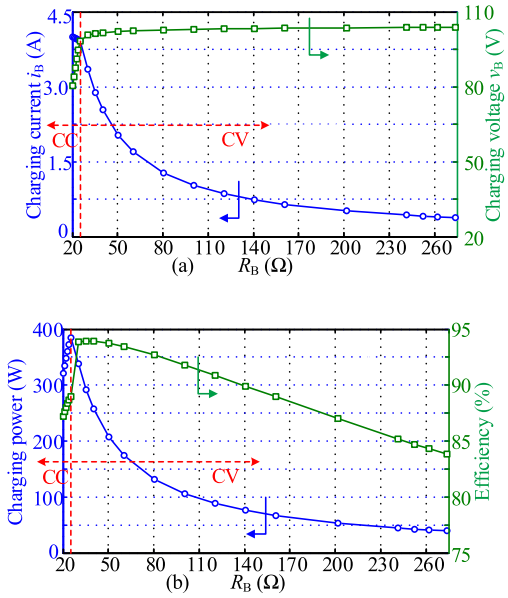

Fig. 13. (a) Charging profile of the electronic load. (b) Efficiency and charging power.

TABLE IV
CALCULATED AND MEASURED POWER LOSSES

Losses distribution	Calculated value		Experimental value	
	CC	CV	CC	CV
Block 1	16.6 W	3.2 W	17.1 W	3.7 W
Block 2	21.3 W	10.3 W	22.9 W	11.2 W
Block 3	7.2 W	7.2 W	7.9 W	7.8 W
Total	45.1 W	20.6 W	47.9 W	22.7 W

current in CC mode is within 2%, and the variation of charging voltage is less than 2.9%, which can meet the requirements of charging. The maximum charging efficiency of the IPT charger is 93.93% in the CV mode.

The calculated and measured power losses in CC and CV modes at $R_B = 25\,\Omega$ are outlined in Table IV, which verify the theoretical model of power losses. The power losses in CC mode is much higher than that in CV mode due to the large reactive power in CC mode.

2) Performance of the Lead-Acid Battery: In this part, the input dc voltage is regulated from 110 to 53 V so that the output voltage/current ($110 - 100\ \mathrm{V}/4\ \mathrm{A} \rightarrow 53 - 48\ \mathrm{V}/1.9\ \mathrm{A}$) can satisfy the requirement of charging a lead-acid battery (48 V/12 AH). The initial charging voltage is 42 V, and the battery voltage gradually increases with charge current 1.9 A in CC mode. Once the voltage hits 48 V, the charging mode switches to the CV mode. Then, the charging current declines until it is smaller than the pre-set value (0.19 A in this paper).

The measured charging profile of the IPT charger is illustrated in Fig. 14(a), which demonstrates that the charging current and charging voltage match the charging profile closely. Fig. 14(b) shows the measured charging efficiencies. There is a rise in efficiency when charging mode alters from CC to CV, the reason for which there is more reactive power in the CC mode than that

TABLE V
COMPARISON WITH METHODS USING CONTROL SCHEMES

Proposed in	Ref. [10]	Ref. [11]	Ref. [12]	Ref. [14]	Ref. [15]	This work
Control scheme	Yes	Yes	Yes	Yes	Yes	No
Number of Component	2+dc-dc converter	2	6	2+dc-dc converter	2+dc-dc converter	6
k	0.3	0.25	0.26	0.26	0.2	0.17
Max. power	9.9 W	5 kW	6.6 kW	600 W	2.9 kW	400 W
Peak efficiency	69.4%	95%	96.1%	82%	88%	93.9%
Frequency (kHz)	140	81.8-88.6	68/79.1	85	20	85

TABLE VI
COMPARISON WITH METHODS USING COMPENSATION TOPOLOGIES

Proposed in		Ref. [9]	Ref. [19]	Ref. [20]	Ref. [21]	Ref. [22]	Ref. [23]	Ref. [24]	This work
Number of inductors		2	1	1	1	1	1	2	1
Number of capacitors		8	2	4	3	5	4	5	4
Number of switches		2	3	2	4	2	2	2	1
Total number		12	6	7	8	8	7	9	6
I_B has design freedom		Yes	No	No	No	Yes	No	Yes	Yes
V_B has design freedom		No	No	Yes	No	No	No	Yes	Yes
Wireless communication		No	Yes	No	No	No	Yes	No	Yes
Number of coils		4	2	2	2	3	3	2	2
Size of coils (mm)	Pri.	400×400	60	150×75	600×600	400	200×100	150×75	400×400
	Sec.	400×400	60	150×75	400×400	200	200×100	150×75	400×400
	Thi.	N/A	N/A	N/A	N/A	400	200×100	N/A	N/A
Gap (mm)		150	10	20	280	200	50	20	150
k		0.17	0.64	0.31	0.1	0.1	0.22	0.31	0.17
Max. power (W)		1000	15	192	150	384	96	216	400
Peak efficiency		93.9%	93%	92.8%	88%	90.8%	91%	91.9%	93.9%
Ave. efficiency		90.8%	90.4%	90.6%	83.3%	83.1%	89.1%	87.3%	88.1%
Frequency (kHz)		85	200	500	50	200	500	500	85

where Pri., Sec., Thi., Max., and Ave. are the abbreviation of the primary coil, secondary coil, third coil, maximum and average, respectively.

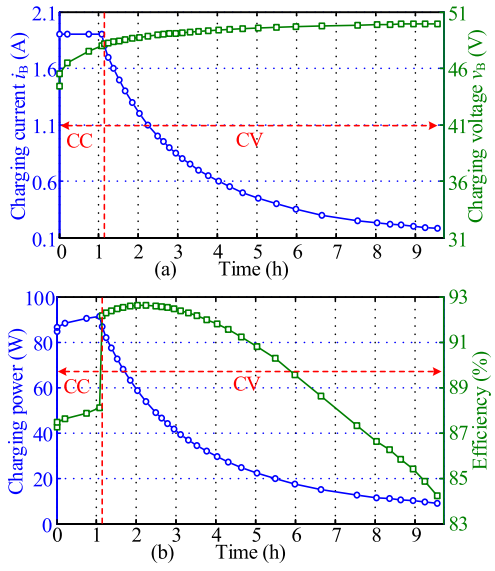

Fig. 14. (a) Charging profile of the lead-acid battery. (b) Efficiency and charging power.

in the CV mode. Moreover, the charging time in the CC mode is much shorter than that in the CV mode.

C. Comparison With Other Methods

The performance of the proposed approach has been compared with other methods 1) using control schemes and 2) using compensation topologies, as outlined in Tables V and VI. Compared with methods using control schemes, the proposed IPT system can realize CC–CV charging without control scheme. Among [10]–[12], [14], and [15], the peak efficiency can reach 96.1% with 6.6 kW [12], while the maximum system efficiency of the proposed IPT charger is lower than that by 2.2% with 400 W. Compared with methods using compensation topologies, the peak efficiency of the proposed system is higher than that of other approaches, but the average efficiency is lower than the maximum average efficiency by 2.7%. However, the proposed IPT charger is superior to the other approaches in terms of the design freedom of charge current/voltage and the number of components.

V. CONCLUSION

In this paper, a VT is proposed for transferring a CC/CV input to a CC or CV output with the help of one ac switch and one capacitor (or inductor). An IPT system with a VT can be applied for CC–CV charging with fewer passive components and ac switches than that of hybrid topologies mentioned in the previous studies. Besides, the VT can let the charge current/voltage of the IPT charger have design freedom with the

constraints of LCT parameters. Moreover, during the derivation of VT, three possible variable parameters of the VT are brought out. For different applications with corresponding requirements, different VTs can be chosen. To verify the theoretical analyses, a 400 W laboratory-scale prototype with the proposed VT for a 100 V/4 A output has been built. Both electronic load and battery are used to test the charging profile of the proposed approach. The experimental results demonstrate that the variation of the charging current in the CC mode is within 2%, and that is less than 2.9% for charging voltage in the CV mode, which is acceptable for battery charging. The measured peak efficiency is 93.93% in the CV mode.

REFERENCES

[1] S. Lee, B. Choi, and C. T. Rim, "Dynamics characterization of the inductive power transfer system for online electric vehicles by Laplace phasor transform," *IEEE Trans. Power Electron.*, vol. 28, no. 12, pp. 5902–5909, Dec. 2013.

[2] W. Li, H. Zhao, S. Li, J. Deng, T. Kan, and C. C. Mi, "Integrated LCC compensation topology for wireless charger in electric and plug-in electric vehicles," *IEEE Trans. Ind. Electron.*, vol. 62, no. 7, pp. 4215–4225, Jul. 2015.

[3] S. Y. Hui, "Planar wireless charging technology for portable electronic products and Qi," *Proc. IEEE*, vol. 101, no. 6, pp. 1290–1301, Jun. 2013.

[4] Y. Jang and M. M. Jovanovi´c, "A contactless electrical energy transmission system for portable-telephone battery chargers," *IEEE Trans. Ind. Electron.*, vol. 50, no. 3, pp. 520–527, Jun. 2003.

[5] R. Mai, Y. Chen, Y. Zhang, N. Yang, G. Cao and Z. He, "Optimization of the passive components for an S-LCC topology-based WPT system for charging massive electric bicycles," *IEEE Trans. Ind. Electron.*, vol. 65, no. 7, pp. 5497–5508, Jul. 2018.

[6] H. Z. Z. Beh, G. A. Covic, and J. T. Boys, "Investigation of magnetic couplers in bicycle kickstands for wireless charging of electric bicycles," *IEEE J. Emerg. Sel. Topics Power Electron.*, vol. 3, no. 1, pp. 87–100, Mar. 2015.

[7] W. Y. Lee, J. Huh, and S. Y. Choi, "Finite-width magnetic mirror models of mono and dual coils for wireless electric vehicles," *IEEE Trans. Power Electron.*, vol. 28, no. 13, pp. 1413–1428, Mar. 2013.

[8] D. H. Tran, V. B. Vu, and W. Choi, "Design of a high-efficiency wireless power transfer system with intermediate coils for the on-board chargers of electric vehicles," *IEEE Trans. Power Electron.*, vol. 33, no. 1, pp. 175–187, Jan. 2018.

[9] Y. Chen, B. Yang, Z. Kou, Z. He, G. Cao, and R. Mai, "Hybrid and reconfigurable IPT systems with high-misalignment tolerance for constant-current and constant-voltage battery charging," *IEEE Trans. Power Electron.*, vol. 33, no. 10, pp. 8259–8269, Oct. 2018.

[10] A. Berger *et al.*, "A wireless charging system applying phase-shift and amplitude control to maximize efficiency and extractable power," *IEEE Trans. Power Electron.*, vol. 30, no. 11, pp. 6338–6348, Nov. 2015.

[11] N. Liu and T. G. Habetler, "Design of a universal inductive charger for multiple electric vehicle models," *IEEE Trans. Power Electron.*, vol. 30, no. 11, pp. 6378–6390, Nov. 2015.

[12] V. Vu, D. Tran, and W. Choi, "Implementation of the constant current and constant voltage charge of inductive power transfer systems with the double-sided LCC compensation topology for electric vehicle battery charge applications," *IEEE Trans. Power Electron.*, vol. 33, no. 9, pp. 7398–7410, Sept. 2018.

[13] C.-S. Wang, G. A. Covic, and O. H. Stielau, "Power transfer capability and bifurcation phenomena of loosely coupled inductive power transfer systems," *IEEE Trans. Ind. Electron.*, vol. 51, no. 1, pp. 148–157, Feb. 2004.

[14] G. Buja, M. Bertoluzzo, and K. N. Mude, "Design and experimentation of WPT charger for electric city car," *IEEE Trans. Ind. Electron.*, vol. 62, no. 12, pp. 7436–7447, Dec. 2015.

[15] Z. Li, C. Zhu, J. Jiang, K. Song, and G. Wei, "A 3-kW wireless power transfer system for sightseeing car supercapacitor charge," *IEEE Trans. Power Electron.*, vol. 32, no. 5, pp. 3301–3316, May 2017.

[16] X. Qu, Y. Jing, H. Han, S. C. Wong, and C. K. Tse, "Higher order compensation for inductive-power-transfer converters with constant-voltage or constant-current output combating transformer parameter constraints," *IEEE Trans. Power Electron.*, vol. 32, no. 1, pp. 394–405, Jan. 2017.

[17] Y. Li, H. Du, M. Yang, and Z. He, "Two-degree-of-freedom H∞ robust control optimization for the IPT system with parameter perturbations," *IEEE Trans. Power Electron.*, vol. 33, no. 12, pp. 10954–10969, Dec. 2018.

[18] W. Zhang and C. C. Mi, "Compensation topologies of high-power wireless power transfer systems," *IEEE Trans. Veh. Technol.*, vol. 65, no. 6, pp. 4768–4778, Jun. 2016.

[19] X. Qu, H. Han, S. C. Wong, C. K. Tse, and W. Chen, "Hybrid IPT topologies with constant current or constant voltage output for battery charging applications," *IEEE Trans. Power Electron.*, vol. 30, no. 11, pp. 6329–6337, Nov. 2015.

[20] R. Mai, Y. Chen, Y. Li, Y. Zhang, G. Cao, and Z. He, "Inductive power transfer for massive electric bicycles charging based on hybrid topology switching with a single inverter," *IEEE Trans. Power Electron.*, vol. 32, no. 8, pp. 5897–5906, Aug. 2017.

[21] C. Auvigne, P. Germano, D. Ladas, and Y. Perriard, "A dual-topology ICPT applied to an electric vehicle battery charger," in *Proc. Int. Conf. Elect. Mach.*, Mar. 2012, pp. 2287–2292.

[22] Y. Li, Q. Xu, T. Lin, J. Hu, Z. He, and R. Mai, "Analysis and design of load-independent output current or output voltage of a three-coil wireless power transfer system," *IEEE Trans. Transp. Electrification*, vol. 4, no. 2, pp. 364–375, Jun. 2018.

[23] Y. Li, J. Hu, F. Chen, S. Liu, Z. Yan, and Z. He, "A new-variable-coil-structure-based IPT system with load-independent constant output current or voltage for charging electric bicycles," *IEEE Trans. Power Electron.*, vol. 33, no. 10, pp. 8226–8230, Oct. 2018.

[24] Y. Chen, Z. Kou, Y. Zhang, Z. He, R. Mai, and G. Cao, "Hybrid topology with configurable charge current and charge voltage output-based WPT charger for massive electric bicycles," *IEEE J. Emerg. Sel. Topics Power Electron.*, vol. 6, no. 3, pp. 1581–1594, Sep. 2018.

[25] Y. Wang, Y. Yao, X. Liu, D. Xu, and L. Cai, "An LC/S compensation topology and coil design technique for wireless power transfer," *IEEE Trans. Power Electron.*, vol. 33, no. 3, pp. 2007–2025, Mar. 2018.

[26] R. W. Erickson and D. Maksimovic, *Fundamentals of Power Electronics*, 2nd ed. Norwell, MA, USA: Kluwer, 2001.

[27] B. X. Nguyen *et al.*, "An efficiency optimization scheme for bidirectional inductive power transfer systems," *IEEE Trans. Power Electron.*, vol. 30, no. 11, pp. 6310–6319, Nov. 2015.

[28] N. Xuan Bac, D. M. Vilathgamuwa, and U. K. Madawala, "A SiC-based matrix converter topology for inductive power transfer system," *IEEE Trans. Power Electron.*, vol. 29, no. 8, pp. 4029–4038, Aug. 2014.

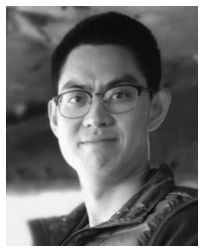

Yang Chen (S'17) received the B.Sc. degree in electrical engineering and automation, in 2015, from the School of Electrical Engineering, Southwest Jiaotong University, Chengdu, China, where he is currently working toward the Ph.D. degree in electrical engineering. In 2018, he received the scholarship under the State Scholarship Fund of China Scholarship Council and became a joint Ph.D. student with the Future Energy Electronics Center (FEEC), Virginia Tech, Blacksburg, VA, USA.

His research interests include wireless power transfer, especially on compensation topology and misalignment tolerance improvement.

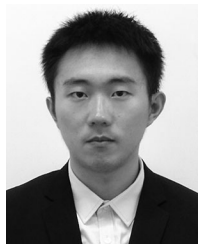

Mingxuan Li received the B.Sc. degree in electrical engineering and automation, in 2017, from the School of Electrical Engineering, Southwest Jiaotong University, Chengdu, China, where he is currently working toward the M.Sc. degree.

His main research interests include wireless power transfer.

Bin Yang received the B.Sc. degree in electrical engineering and automation from the School of Electrical and Automation Engineering, East China Jiaotong University, Nanchang, China, in 2017. He is currently working toward the M.Sc. degree at the School of Electrical Engineering, Southwest Jiaotong University, Chengdu, China.

His main research interests include wireless power transfer.

Shuxin Chen (S'17) received the B.Eng. degree in electronic engineering from the Hong Kong Polytechnic University, Hong Kong, in 2015, the bachelor's degree in microelectronic engineering from the Sun Yet-Sen University, Guangzhou, China, in 2015, and the M.Sc. degree in power engineering from Nanyang Technological University, Singapore, in 2016. He is currently working toward the Ph.D. degree in electrical and electronic engineering at Nanyang Technological University.

His current research interests include wireless power transfer and power converter control.

Qiao Li received the B.Sc. degree in electrical engineering and automation from the College of Nuclear Technology and Automation Engineering, Chengdu University of Technology, Chengdu, China, in 2017. He is currently working toward the M.Sc. degree at the School of Electrical Engineering, Southwest Jiaotong University, Chengdu.

His main research interests include wireless power transfer.

Zhengyou He (M'10–SM'13) received the B.Sc. and M.Sc. degrees in computational mechanics from Chongqing University, Chongqing, China, in 1992 and 1995, respectively, and the Ph.D. degree in power system and automation from the School of Electrical Engineering, Southwest Jiaotong University, Chengdu, China, in 2001.

He is currently a Professor with the School of Electrical Engineering, Southwest Jiaotong University. His research interests include signal process and information theory applied to electrical power system and application of wavelet transforms in power system.

Ruikun Mai (M'14) received the B.Sc. degree in electronic and information engineering and the Ph.D. degree in power system and automation from Southwest Jiaotong University, Chengdu, China, in 2004 and 2010, respectively.

He is currently a Professor with the School of Electrical Engineering, Southwest Jiaotong University. His research interests include wireless power transfer and its application in railway systems, power system stability and control.